

Reprinted from

PHYSICS LETTERS A

Physics Letters A 253 (1999) 16-20

Increased thermal noise in nonuniform fiber suspensions

Phil Willems¹, Mukund Thattai²

LIGO Project, California Institute of Technology 18-34, Pasadena, CA 91125, USA

Received 11 November 1998; revised manuscript received 18 December 1998; accepted for publication 29 December 1998
Communicated by P.R. Holland



LIGO-P980014-00-D

factor, which is the ratio of the gravitational energy of the suspension pendulum motion to its elastic energy. Since the suspension loss is due entirely to the elastic loss (assuming all other losses, such as residual gas damping, are eliminated by careful design), the loss of the pendulum is just the intrinsic loss divided by the dilution factor.

The elastic energy of a wire pendulum is in turn a function of the wire diameter. The thinner the wire, the less stiff it is and the less elastic energy it stores during the pendulum oscillation. The gravitational energy is independent of the wire diameter except through its mass, which is ignorably small compared to the mirror test mass. The gravitational energy does increase linearly with the wire length; therefore, a low loss pendulum should be as long as possible to maximize gravitational energy, and as thin at its endpoints as possible to minimize elastic energy, consistent with safely supporting the test mass mirror ($S_{\max} = mg/n\pi r^2$ where m is the mirror mass, r is the fiber radius and there are n suspension wires). Excess noise motion of the test mass due to creep in highly stressed suspension wires may also set a lower limit to the wire radius.

It is here that the manufacturing process of fused silica fibers interferes with their function, because it is precisely at the fiber endpoints that the diameter is increasing. This paper presents calculations of the reduction of the dilution factor due to the taper regions at the fiber endpoints.

2. The physical model

The physical system modelled for this analysis is a single wire pendulum similar to that modelled by González and Saulson [11]. A single wire of length L is rigidly attached at its top end to a fixed support and supports a mirror of mass M and moment of inertia J at its bottom end. The wire has linear mass density $\rho(z)$ and moment of inertia $I(z)$ that are functions of position along the wire length; the tension $T = Mg$ is approximated as constant along the wire. The wire is rigidly attached to the mirror at a distance h above the mirror's center of gravity. Only motion in the x -direction, perpendicular to the mirror face, is considered.

Taking $x_M = x(L) + hx'(L)$ and $\Phi = x'(L)$ as the position and rotation of the test mass mirror, respec-

tively, the equations of motion for such a single wire pendulum are:

$$-E[I(z)x^{iv}(z) + 2I'(z)x'''(z) + I''(z)x''(z)] + Tx''(z) = \rho(z)\ddot{x}(z), \quad (1)$$

$$E[I'(L)x''(L) + I(L)x'''(L)] - Tx'(L) = M\ddot{x}_M, \quad (2)$$

$$-E[hI(L)x'''(L) + \{hI'(L) + I(L)\}x''(L)] = J\ddot{\Phi}, \quad (3)$$

along with the boundary conditions $x(0) = x'(0) = 0$ at the top of the fiber. These equations differ from those of González and Saulson in the presence of additional terms describing the variation of I and ρ with z ; the derivation is a straightforward extension to the one they present. The mechanical loss of the system enters the equations through the imaginary part of the complex Young's modulus E of the fiber.

These additional terms render these equations generally unsolvable by analytic means, so we solved them numerically using a finite-element analysis. A sinusoidal driving force was added to Eq. (2). We modelled the wire as a finite mesh of a few thousand discrete points, thus reducing the complex fourth-order differential Eq. (1) to a set of eight coupled first-order difference equations for each point on the mesh. We then iteratively improved an initial guess at the solution to $x(z)$ into conformance with the difference equations and boundary conditions using a relaxation technique [12]. The response of the pendulum test mass mirror as a function of drive frequency then determined the thermal noise spectrum and the Q -values of the system's resonant modes.

We tested the program performing these calculations by comparing its results for the uniform wire pendulum to the exact analytic solution. The two methods yielded the same answers for the mode shapes, frequencies, and Q -values for the first several modes of the system. The two techniques also agreed on the strength and slope of the background thermal noise spectrum. The numerical calculations also showed the Q of the modes to be inversely proportional to the intrinsic loss, as expected.

The geometry of actual fiber tapers will depend on the details of their fabrication and can be expected to vary between techniques of manufacture. For the sake of concreteness, we have considered three par-

ticular types of taper: linear, exponential, and inverse-square-root. All three are experimentally realizable in the laboratory, and should apply in varying degrees to actual fibers in the laboratory. The exponential taper is created by pulling the fiber in a uniform hot zone of constant width, and has the profile:

$$r(z) = r_0 \exp\left(-\ln\left(\frac{r_0}{r_1}\right) \frac{z}{z_0}\right), \quad (4)$$

where r_0 is the radius of the end piece, r_1 is the radius of the flexible inner region of the fiber, and z_0 is the taper length. The inverse-square-root taper is expected in a fiber drawn in a tower with a uniform hot zone, and has the profile:

$$r(z) = r_0 / \sqrt{1 + \left(\left(\frac{r_0}{r_1}\right)^2 - 1\right) \frac{z}{z_0}}. \quad (5)$$

The linear taper is produced by pulling a fiber in a uniform hot zone with width that decreases at half the rate at which the fiber is pulled:

$$r(z) = r_0 - (r_0 - r_1) \left(\frac{z}{z_0}\right). \quad (6)$$

This last geometry is somewhat more difficult to achieve but has been shown in the laboratory [13]. Though somewhat arbitrary, these taper profiles are useful in displaying trends that more general tapers will obey; in addition, there is nothing to prevent experimentally measured taper geometries from being modelled in the program as they become available.

3. Results of the simulation

The fiber pendulum that we modelled for the nonuniform case was chosen to have parameters similar to that used by Rowan et al. [8], the major difference being that our mass was chosen to be half as heavy as theirs since they used a two-wire pendulum instead of our one-wire pendulum and we wished to keep the wire diameters and tensions similar.

We find that, for the set of taper geometries considered, the reduction in the dilution factor can be as much as a factor of two, with even greater reductions possible for more extreme tapers. One way to show this is to take the overall length of the fiber as fixed, as well as the diameters of the flexible region of the

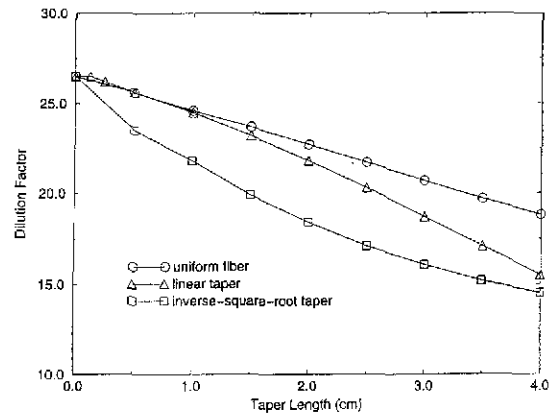


Fig. 1. Dilution factor vs. taper length. The fiber parameters are: length 30 cm, inner diameter 290 μm , outer diameter 3 mm. The data for the exponential taper are very close to those for the linear taper and so are not shown.

fiber and the end pieces, and examine the change in the dilution factor as the length of the taper region is increased from zero. The results of these calculations are shown in Fig. 1.

The Q of even a uniform wire pendulum is expected to vary with length according to the approximate formula [11]

$$\frac{1}{Q} = \frac{1}{Q_{\text{mat}}} \times \frac{2}{kL} \left(1 + \frac{(n\pi)^2}{2kL}\right), \quad (7)$$

where k is the elastic wavenumber of the fiber and is a function of the fiber diameter and n is the number of the mode of the system being studied. For the lowest modes of the system, $kL \gg 1$, so for the first violin mode studied here Q will increase linearly with L . A naive model of the system would assume that the length of the pendulum is just the length of the uniform part of the fiber between its taper regions, and that the dilution factor and mode frequency are given by a uniform pendulum of this dimension. The data show that the effective length is always longer than this for nonzero tapers, and so at least part of the taper region flexes during oscillation, leading to increased mechanical loss. Data showing the frequency of the first violin mode as a function of taper length are shown in Fig. 2. Notice that the inverse-square-root taper shows the least increase in frequency, and the largest increase in loss. This is because the inverse-square-root taper concentrates most of its diameter change close to the end of the fiber. The rest of the taper is gradual, and

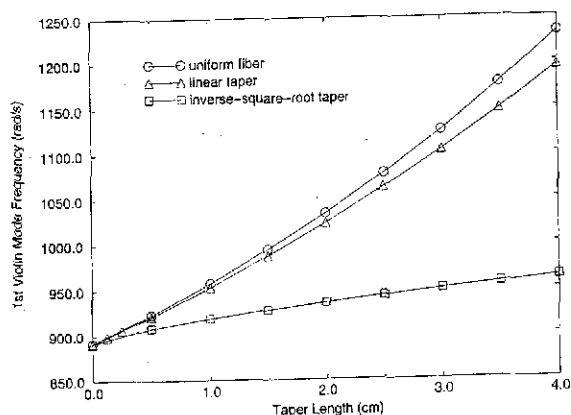


Fig. 2. Frequency of the first violin mode vs. taper length. The fiber parameters are the same as in Fig. 1.

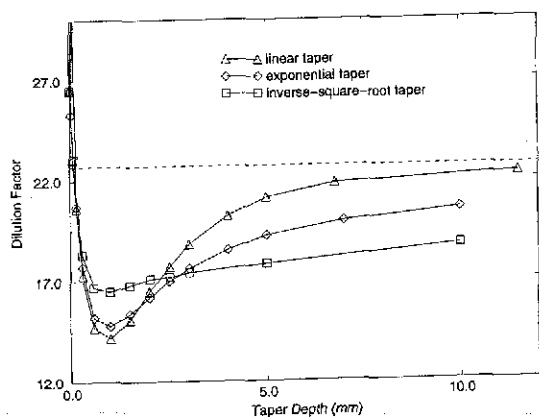


Fig. 3. Dilution factor vs. taper depth. The parameters of the fiber are: fiber length 30 cm, inner diameter $290 \mu\text{m}$, taper length 2 cm.

thus relatively flexible despite its increasing diameter, causing a large loss increase.

This behavior is seen in the second set of calculations, where the length of the taper and the inner fiber diameter were held fixed, and the diameter of the end regions was allowed to vary (Fig. 3). When the difference between the inner and outer diameters goes to zero, all three tapers reduce to a uniform fiber. As the difference between the inner and outer diameters becomes very large, the taper transition becomes very abrupt, and the behavior of the fiber approaches that of a uniform fiber of the shorter length between the tapers, as the dilution factor data show. However, there is a taper depth where the Q becomes a minimum of about half the Q of the uniform fiber. This is true for all three taper types, which resemble each other closely

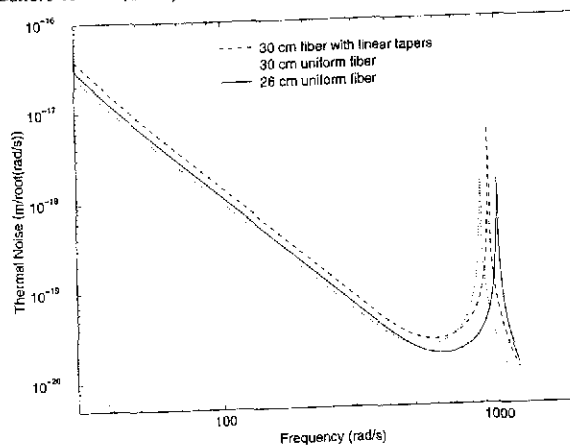


Fig. 4. Thermal noise spectra of tapered and untapered fiber pendulums. The broadband thermal noise spectrum is 40% higher for the tapered fiber, which has taper length 2 cm and taper depth 1 mm. The loss fraction is 10^{-7} .

when the outer diameter is not much larger than the inner diameter. This occurs when the increase in diameter is not large enough to exclude bending but is large enough to induce excess loss. As the outer diameter increases further, the taper becomes too stiff to bend and the losses decrease.

The data at very large taper depths must be considered with some skepticism, for the equations of motion are based upon the assumption that the cone angle made by the axial tangent to the fiber surface is small, which is not obviously the case for taper depths as large as 10 mm in these calculations, where the cone angle is $\sim \arctan(\frac{1}{2}) = .46$. However, the trends are intuitively reasonable, and the most drastic reductions in Q are at small taper depths, where the model is expected to be most accurate.

4. Conclusions

As expected, the reduction in Q for the resonant modes of the system is accompanied by a corresponding increase in the off-resonant thermal noise (see Fig. 4). For the worst case shown above, the thermal noise in the gravitationally interesting 5–100 Hz range is increased by a factor of 1.4 over the uniform fiber case. It must be remembered that the worst case shown here is not necessarily the worst possible case; longer, more gradual tapers can be expected to produce even larger increases. The presence of tapers must therefore be considered a potentially important noise source.

The solutions suggested by this analysis are relatively simple to implement, however. The best Q 's are obtained by giving the taper the largest possible linear slope at the point near the uniform region. Therefore, tapers should be short, end in a large diameter relative to the uniform region, and have linear- or exponential-like profiles. Fabricating fibers with small hot zones would be one approach, perhaps using a carbon dioxide laser to heat the fiber rather than a hydrogen torch. Another way would be to use tailored torch oscillation routines as described by Birks and Li [13] to achieve more desirable taper profiles. A third way would be to dispense with the tapers altogether and weld the uniform parts of the fiber directly into the suspension.

Acknowledgement

The authors wish to thank Yuri Levin, Gabriela Gonzalez, Sheila Rowan, Vladimir Braginsky, and Peter Saulson for useful discussion. This work was supported by the National Science Foundation under grant

NSF PHY-9700601. Mukund Thattai acknowledges the Caltech SURF program for support during this work.

References

- [1] R.E. Vogt et al., A laser interferometer gravitational-wave observatory (LIGO), Proposal to The National Science Foundation (1989).
- [2] K. Danzmann et al., GEO 600: Proposal for a 600 m laser interferometric gravitational wave antenna, Max-Planck-Institut für Quantenoptik Report 190, Garching (1994).
- [3] A. Brillet et al., VIRGO final conceptual design (1992).
- [4] H.B. Callen, T.A. Welton, *Phys. Rev.* 83 (1951) 34.
- [5] S. Traeger et al., *Phys. Lett. A* 225 (1997) 39.
- [6] V.B. Braginsky et al., *Phys. Lett. A* 218 (1996) 164.
- [7] V.B. Braginsky et al., *Physics-Doklady* 40 (1997) 564.
- [8] S. Rowan et al., *Phys. Lett. A* 233 (1997) 303.
- [9] S. Rowan et al., *Phys. Lett. A* 227 (1997) 153.
- [10] S. Rowan et al., *Class. Quantum Grav.* 14 (1997) 1537.
- [11] G. González, P. Saulson, *J. Acoust. Soc. Am.* 96 (1994) 207.
- [12] W.H. Press et al., *Numerical Recipes in C*, 2nd Ed. (Cambridge Univ. Press, New York, 1992).
- [13] T.A. Birks, Y.W. Li, *J. Lightwave Tech.* 10 (1992) 432.